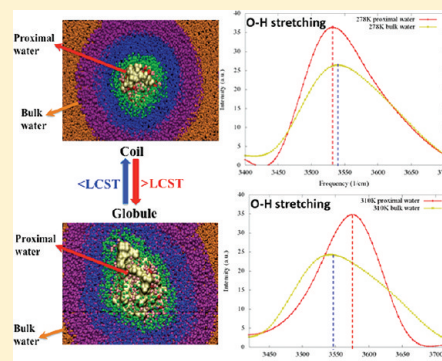


Vibrational Spectra of Proximal Water in a Thermo-Sensitive Polymer Undergoing Conformational Transition Across the Lower Critical Solution Temperature

Sanket A. Deshmukh,[†] Subramanian K. R. S. Sankaranarayanan,^{*,†} and Derrick C. Mancini^{*,†,‡}

[†]Center for Nanoscale Materials and [‡]Advanced Photon Source, Argonne National Laboratory, Argonne, Illinois 60439, United States

ABSTRACT: The vibrational spectrum of water near a thermo-sensitive polymer poly(*N*-isopropylacrylamide) (PNIPAM) undergoing conformational transition through the lower critical solution temperature (LCST) is calculated using molecular dynamics simulations. The characteristic structural features observed at the atomic scale for these proximal water molecules in a solvated polymer chain while undergoing the conformational transition are strongly correlated to their vibrational densities of states. Comparison of the vibrational spectrum below LCST for the proximal water with the vibrational spectrum obtained for bulk water reveals a significant fraction of the hydrogen bonding between the proximal water molecules and the polymer side groups. Hydrogen-bonded bridges of water molecules are formed between two adjacent and alternate monomers. This network of hydrogen bonding results in formation of locally ordered water molecules at temperatures below the LCST. Analysis of the simulation trajectories confirms the presence of a quasi-stable solvation structure near the PNIPAM. The calculated vibrational spectra for proximal water above the LCST suggest significantly reduced hydrogen bonding with the polymer and indicate a reduction in the structural stability of proximal water around a collapsed polymer chain. Systematic trends in the observed peak intensities and frequency shifts at the low- and high-frequency ends of the spectrum can be correlated with the structural and dynamical changes of water molecules below and above the LCST transition, respectively, for various polymer chain lengths. The simulations reveal that, compared to bulk water, the libration bands are blue shifted and OH stretch bands red shifted for water in proximity to PNIPAM with 30 monomer units below the LCST. The simulations suggest that vibrational spectra can be used as a predictive tool for quantifying atomic-scale structural transitions in solvation of thermo-sensitive polymers such as PNIPAM.



I. INTRODUCTION

Although the thermodynamic and structural properties of bulk water are well known, the complex intermolecular forces that govern its nanoscopic structural arrangements and dynamics have made a detailed atomistic picture of the instantaneous local structures of water and their structural evolution elusive.^{1–4} “Proximal water” represents water molecules located near surfaces and interfaces or in the vicinity of a molecule such as a polymer chain in solution. The behavior of proximal water molecules is of fundamental interest in biology, materials science, environmental science, geochemistry, and heterogeneous catalysis.^{5–10} In particular, these effects are known to occur at short distances from the aqueous media–material boundary and can have a profound effect on the dynamical processes occurring at an atomistic scale. For example, the properties of proximal water at the solid–liquid interface plays an important role in several processes, which includes ion adsorption/desorption on surfaces and ion diffusion in nanopores, biological membranes, and ion channels.^{11–14} It is therefore not surprising that the study of the atomic-scale structure of proximal water continues to be a subject of immense scientific interest.

There are several problems, including protein folding, wetting, corrosion, membrane function, environmental pollu-

tion, and soil weathering, where proximal water molecules play an essential role.^{15–19} For example, it plays a key role in governing the structure, stability, dynamics, and functionality of proteins due to the dynamical coupling that exists between these water molecules and the protein. Atomistic information of such coupling is necessary to understand the role played by proximal water during biological processes, such as protein–substrate binding, folding–unfolding phenomena, etc.^{20–23} A similar argument also holds true for other complex polymeric materials such as hydrogels that are of great importance in several fields including controlled drug delivery systems.²⁴ The structure and dynamics of proximal water dictates the transport phenomena at the nanoscale and plays a key role in keeping the hydrogel solvated.²⁵ Despite its importance in several areas of science, the atomic-scale characterization and information regarding the proximity effects and the structure and dynamics of proximal water in solvated ionic polymers such as proteins and hydrogels is still lacking. This is primarily attributed to their complex structure, which makes it difficult to deconvolute the measured vibrational and optical spectra.^{20–23}

Received: December 8, 2011

Revised: April 9, 2012

Published: April 10, 2012

The PNIPAM–water system represents a relatively simple representative model of an ionic polymer where knowledge of the proximal water structure is crucial for elucidating fundamental physical phenomena such as the polymer conformational transformations, which eventually dictate its functional properties.^{26,27} PNIPAM is a thermo-sensitive polymer, and solution of PNIPAM shows an LCST at \sim 305 K.²⁸ The molecular conformational transitions are strongly correlated to the dynamical processes at the atomistic level that occur at the polymer–water interface in solution. Typically, what drives coil-to-globule transformations is an uncommonly large entropy change, which has been attributed to an enhanced restructuring of water in the immediate vicinity of the polymer.²⁸ Figure 1 shows the schematic of the nature and

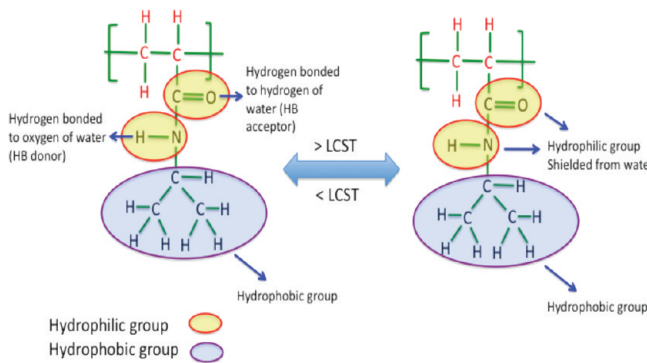


Figure 1. Schematic showing changes in the hydrophilic nature of acceptor and donor sites of PNIPAM during the conformational transition across the LCST.

extent of hydration of a monomer unit of PNIPAM both below and above the LCST. Below the LCST, both the acceptor and the donor groups of PNIPAM form hydrogen bonds with water molecules. The hydrophobic group of PNIPAM, however, cannot form a hydrogen bond with water molecules, which results in formation of a cage-like structure of water molecules around the PNIPAM.²⁸ Increasing the temperature makes some of the hydrophilic groups (acceptor and donor sites) shielded from water, which leads to a phase separation of PNIPAM and water.

Atomic-scale insights into the dynamics and structural transformation of the proximal water and its role in inducing polymer collapse through the LCST remain a fundamental and challenging problem in polymer science.²⁸ An important question that arises in this regard is how to characterize the changes in the local solvent structure and its effect on the conformation transitions of the short-chain-length oligomers at the atomistic level.

Experimental techniques such as surface-specific sum-frequency vibrational spectroscopy (SFVS)^{29–32} and total internal reflection (TIR) sum-frequency vibrational spectroscopy (VSFS)³³ have been employed to gain insights into the structure of water near surfaces. These methods have helped identify ice-like, liquid-like, and dangling O–H structures in the terminated hydrogen-bonding network of the water layer located in close proximity to air–water, aqueous–organic, and water–quartz interfaces.^{34–36} Far less is known, however, about the structure and dynamics of proximal water in aqueous polymer systems in which the polymer can undergo a conformational transition with a change in its environment such as temperature or pH. A detailed understanding of the

molecular-scale structure is necessary to exercise control over the dynamical processes occurring in the proximal water.

Experimental measurements that can provide a detailed atomistic view of the structure of proximal water and the nature of its hydrogen bonding have been found to be problematic due to the difficulty in selectively probing the proximal water molecules.³³ This is especially true for aqueous solutions of polymers in which short-chain-length oligomers undergo rapid fluctuation in the radius of gyration (R_g).³⁷ Also, for these systems, the network of hydrogen-bonded water molecules is highly dynamic and time-resolved vibrational spectroscopy studies in the picoseconds and subpicosecond time scales would be required to understand the ultrafast vibrational dynamics of proximal water and characterize the atomic-scale structural changes.

Theoretical studies provide an aid to understanding the dynamics and molecular structure of proximal water for aqueous polymers.^{26,27} In particular, molecular dynamics (MD) is a powerful tool that can be used to simulate the structure of proximal water in solvated polymers at an atomistic level.^{12,27} MD simulations have been previously used to classify hydrogen bonds and spectra for molecules in different hydrogen-bonding states.^{12,27} There are very limited theoretical studies that have focused on characterization of the structure of water at the interface of polymers.^{27,38–44} Though these studies have captured structural changes in water, atomic-scale characterization of proximal water associated with conformational variation in polymers while accounting for solvent effects is still lacking. The existing models do not explicitly account for direct electrostatic interactions between solvent and polymer, for the local arrangement of solvent molecules around the polymer chain, and for formation of hydrogen bonds between the solvent and the monomer units.

In this work, we attempted to provide better understanding and characterization of the structure of proximal water in a solvated polymer that undergoes a conformational transition. We employ an all-atom MD simulation that probes the local structure and dynamics of proximal water near a single polymer chain of PNIPAM. Specifically, we focus on the vibrational spectroscopy of the proximal water below and above the LCST of PNIPAM, namely, at 278 and 310 K. In this work, we mainly focused on the high-frequency region ($>3000\text{ cm}^{-1}$) of the vibrational spectra that represents the O–H stretching band. The O–H stretching band of the proximal water is known to experimentally show a red shift because of the presence of the strong hydrogen bonds between the hydrophilic groups of PNIPAM and water below the LCST compared to above the LCST of PNIPAM.⁴⁵ To this end, we studied the temperature-sensitive polymer PNIPAM using MD simulation below and above the LCST of PNIPAM (at 278 and 310 K, respectively) in isothermal-isobaric ensembles (NPT) at 1 atm pressure. PNIPAM chains consisting of 5 monomers (5-mer) and 30 monomers (30-mer) were studied in the presence of water molecules using a polymer-consistent force field (PCFF).⁴⁶ The experimental work of Ahmed et al. defines a “persistent length” for the PNIPAM polymer chains to show an LCST.⁴⁷ They identified a characteristic length of \sim 10 monomers; polymer chains above this length undergo a coil-to-globule conformational transition above the LCST, whereas those below the persistent length do not undergo the transition.⁴⁷ Accordingly, we simulated the 5-mer and 30-mer, which represent two different polymer chain lengths below and above the persistent length, respectively.

Table 1. PCFF Parameters for the Water Model

quartic polynomial for bond stretching				
bonds	b_0 (Å)	K_2 (kcal·mol ⁻¹ ·Å ⁻²)	K_3 (kcal·mol ⁻¹ ·Å ⁻³)	K_4 (kcal·mol ⁻¹ ·Å ⁻⁴)
O–H	0.9700	563.2800	-1428.2200	1902.1200
quartic polynomial for angle bending				
bond angles	θ_0 (deg)	H_2 (kcal·mol ⁻¹ ·deg ⁻²)	H_3 (kcal·mol ⁻¹ ·deg ⁻³)	H_4 (kcal·mol ⁻¹ ·deg ⁻⁴)
H–O–H	0.9700	49.8400	-11.6000	-8.000
nonbonded van der Waals interactions				
bond angles		σ (Å)	ϵ (kcal·mol ⁻¹)	
O		3.6080	0.27400	
H		1.0980	0.1300	

II. COMPUTATIONAL DETAILS

II.a. Potential Model. The all-atom model of PNIPAM and water has been used to study the vibrational spectra of water. The accuracy of the MD simulations depends on the choice of the force field. The polymer-consistent force field (PCFF) has

been successfully used in the past to carry out MD simulation of different polymer and water systems.⁴⁸ In this work, we used a polymer-consistent force field (PCFF) with its form given by eq 1.⁴⁶

$$\begin{aligned}
 E_{\text{pot}} = & \sum_b [K_2(b - b_0)^2 + K_3(b - b_0)^3 + K_4(b - b_0)^4] + \sum_\theta H_2(\theta - \theta_0)^2 + H_3(\theta - \theta_0)^3 + H_4(\theta - \theta_0)^4 \\
 & + \sum_\phi [V_1[1 - \cos(\phi - \phi_1^0)] + V_2[1 - \cos(2\phi - \phi_2^0)] + V_3[1 - \cos(3\phi - \phi_3^0)]] \\
 & + \sum_x K_x x^2 + \sum_b \sum_{b'} F_{bb'}(b - b_0)(b' - b'_0) + \sum_\theta \sum_{\theta'} F_{\theta\theta'}(\theta - \theta_0)(\theta' - \theta'_0) + \sum_b \sum_\theta F_{b\theta}(b - b_0)(\theta - \theta_0) \\
 & + \sum_b \sum_\phi (b - b_0)[V_1 \cos \phi + V_2 \cos 2\phi + V_3 \cos 3\phi] + \sum_{b'} \sum_\phi (b' - b'_0)[V_1 \cos \phi + V_2 \cos 2\phi + V_3 \cos 3\phi] \\
 & + \sum_\theta \sum_\phi (\theta - \theta_0)[V_1 \cos \phi + V_2 \cos 2\phi + V_3 \cos 3\phi] + \sum_\phi \sum_\theta \sum_{\theta'} K_{\phi\theta\theta'} \cos \phi (\theta - \theta_0)(\theta' - \theta'_0) + \sum_{i>j} q_i q_j \cdot \frac{1}{\epsilon r_{ij}} \\
 & + \sum_{i>j} [(A_{ij}/r_{ij}^9) - (B_{ij}/r_{ij}^6)] \\
 \end{aligned} \tag{1}$$

In eq 1, terms 1, 2, 3, and 4 are the bond stretching, angle bending, dihedral, and out-of-plane (also called inversion) terms, respectively. b is the bond length during simulations, b_0 is the equilibrium bond length of the bond, and K_2 , K_3 , and K_4 are the corresponding force constants for bonds. θ and θ_0 are the observed angle during simulations and equilibrium angle, respectively, and H_2 , H_3 , and H_4 are the corresponding force constants. Similarly, ϕ_0 and ϕ are the equilibrium dihedral angle and dihedral angle during the simulations, respectively, and V_1 , V_2 , and V_3 are the corresponding force constants. The out-of-plane angle is given by χ , and K_χ is the corresponding force constant. Terms 5–11 define the cross interactions which include the dynamic variations among the bond stretching, bending, and torsion angle rotation. The force constant for the cross term between two bonds with one common atom is given by $F_{bb'}$. $F_{\theta\theta'}$ refers to the force constant for the two angles with a common bond, and $F_{b\theta}$ is the force constant for the cross term between a bond and an angle in which the bond is one of the edges. The last two terms, 12 and 13, describe the Coulombic electrostatic force and van der Waals interactions, respectively. r_{ij} is the distance between two atoms i and j . q_i and q_j are the charges on atoms i and j . ϵ is the dielectric constant. Numerical

values of the various force-field parameters are available in refs 49 and 50. A PCFF water model, with a partial charge of -0.798 on the oxygen atom and +0.399 on the hydrogen atom, was used in all simulations.⁴⁸ Table 1 shows the parameter details for the PCFF water model.

II.b. MD Simulation Details. In the initial step of structure generation a monomer unit of PNIPAM was generated and repeated to generate isotactic-rich chains of PNIPAM of different chain lengths. One end of PNIPAM was terminated with a CH_3 group and the other with a hydrogen atom. The all-atom model of PNIPAM consisting of 5-mer and 30-mer was thus generated and placed in the cubic simulation cell. These chains were equilibrated for 100 ps. This relaxation was followed by random insertion of the PCFF water molecules. The initial water density was chosen to be close to that of bulk water, $\sim 1 \text{ g/cm}^3$. Simulations were then carried out for a total of 20 ns. Eighteen nanoseconds of the 20 ns were considered as the production run, and atomic trajectories of last 18 ns were considered for all dynamical analysis. Systems studied are listed in Table 2.

To study the structural evolution of polymer and water across the LCST, simulations were conducted in NPT (moles

Table 2. System Details Employed in This Study

system	no. of PNIPAM monomers	no. of waters	density (g/cm ³) (after relaxation of 2 ns)
A	5	1200	1.026
B	30	9000	1.025

(N), pressure (P), and temperature (T) are conserved) ensembles at 278 and 310 K at 1 atm pressure. A Nose–Hoover barostat and thermostat was used to maintain the pressure and temperature with time constants of 1 and 2 ps, respectively. The LAMMPS simulation package was used to carry out all simulations with periodic boundary conditions with a LJ cutoff of 9.5 Å for all nonbonded interactions.⁵¹ Long-range electrostatic interactions were calculated by the Ewald summation method. A time step of 1 fs was used to carry out the simulation of 20 ns. Atomic trajectories (atom positions, temperature, pressure, velocities etc.) were accumulated and stored every 1 ps. Trajectory files obtained from these simulations were analyzed for various structural and dynamical properties.

Radial distribution functions (RDFs) were calculated to determine the difference in the structural arrangements of polymer and water at 278 and 310 K. RDFs between the carbon atoms in the backbone of PNIPAM and the oxygen atom of water were evaluated to study the effect of temperature on the local ordering of water molecules in a solvated polymer. Additionally, RDF of the key atom pairs that are involved in hydrogen bonding, namely, carbonyl oxygen (op) and hydrogen (hw) atoms of water, was calculated to evaluate the effect of temperature. RDF for oxygen atom of water with itself was also calculated at 278 and 310 K.

To study the structural evolution in PNIPAM at 278 and 310 K, the radius of gyration (R_g) was calculated for both 5-mer and 30-mer. The instantaneous R_g , which is a measure of the size of a group of oligomer, was calculated for each frame of atomic trajectory using eq 2

$$R_g^2 = \frac{1}{M} \sum_i m_i (r_i - r_{cm})^2 \quad (2)$$

where r_{cm} is the center of mass position of the group, M is the mass of the group, and the sum is over all atoms in the group.

The self-diffusion coefficient for proximal water, bulk water, and PNIPAM with 5-mer and 30-mer was calculated to study the diffusive properties of PNIPAM at 278 and 310 K. The self-diffusion coefficient was calculated using Einstein's relation between the self-diffusion coefficient and the mean square displacement (MSD).⁵² This relation is given as

$$6D_t = \lim_{t \rightarrow \infty} \langle (r(t) - r(0))^2 \rangle \quad (3)$$

where $\langle (r(t) - r(0))^2 \rangle$ is the MSD and $r(t) - r(0)$ is the displacement vector of a penetrant that occurs in time t . The angular brackets denote an ensemble average over all penetrants in the system and all time origins. D_t is obtained from the linear slope of the MSD at longer times.

A literature survey on the coil-to-globule transition of PNIPAM suggests that interactions between water and polymer play a very important role in defining the coil-to-globule transition.^{53,54} We therefore evaluated the hydrogen-bonding characteristics of water and PNIPAM with 5-mer and 30-mer at 278 and 310 K. The following geometric criteria was used to

represent hydrogen bonding between a pair of water molecules^{55,56}

$$\begin{aligned} R_{OO} &\leq 3.6\text{\AA} \\ R_{OH} &\leq 2.45\text{\AA} \\ \phi &\leq 30^\circ \end{aligned} \quad (4)$$

In the above equation, R_{OO} represents the distance between oxygen and oxygen atoms of water 1 and 2. R_{OH} is the distance between the oxygen and the hydrogen atoms of water 1 and water 2, which form the hydrogen bond. The angle ϕ is the angle between the oxygen atom of water 1 and the oxygen and hydrogen atoms of water 2 ($O_1\cdots O_2-H_2$). This geometric criteria fulfills the potential energy requirements that are typical for hydrogen bonds.^{57,58} In this study, the first minimum in the corresponding radial distribution functions of pure water was chosen as the cutoff distances, R_{OO} and R_{OH} . Similar geometric criteria were used to define the hydrogen bond between water and polymer. Two types of polymer–water hydrogen bonds that are possible in this system are the bond between (1) the carbonyl oxygen atom (op) and the water hydrogen atom (hw) and (2) the hydrogen atom of the amide group (hp) and the water oxygen atom (ow).

A hydrogen-bond occupation number (S_{ij}) can be defined to distinguish between the hydrogen-bonded and non-hydrogen-bonded atoms.

hydrogen-bond occupation number (S_{ij})

$$= \begin{cases} 1 & (\text{hydrogen bonded}) \\ 1 & (\text{non-hydrogen bonded}) \end{cases}$$

The stability of the hydrogen bonds was determined by defining a time-dependent autocorrelation function of this state variable S_{ij} that describes the existence or nonexistence of bonds between a selected donor–acceptor pair ij (eq 5). Two types of correlation functions can be defined: intermittent and continuous.^{59,60} In the case of continuous correlation, the hydrogen-bond occupation number (S_{ij}) is allowed only one transition from 1 to 0 when the bond between atom i and atom j breaks for the first time. After the first breakage of hydrogen bonds between atom i and atom j , S_{ij} was never allowed to return to 1. In the case of intermittent correlation, $S_{ij}(t + t_0)$ was set to 1 if the bond between atom i and atom j was found to be present in the time steps t_0 and $t_0 + t$, irrespective of whether it is broken or reformed at intermediate times

$$C_x(t) = \left\langle \frac{\sum_{ij} S_{ij}(t + t_0) \cdot S_{ij}(t_0)}{\sum_{ij} S_{ij}(t_0) \cdot S_{ij}(t_0)} \right\rangle \quad (5)$$

where $x =$ a continuous (c) or intermittent (i) autocorrelation function.

Vibrational spectra were calculated by Fourier transforming of the atomic velocity autocorrelation function (VAF) obtained from the MD simulation trajectories. They provide the density of states (DOS) spectral frequencies characteristic of various intramolecular vibrational modes. Equation 6 gives the expression for the vibrational spectra

$$G(\omega) = \int_{-\infty}^{\infty} VACF \exp(-i\omega t) dt \quad (6)$$

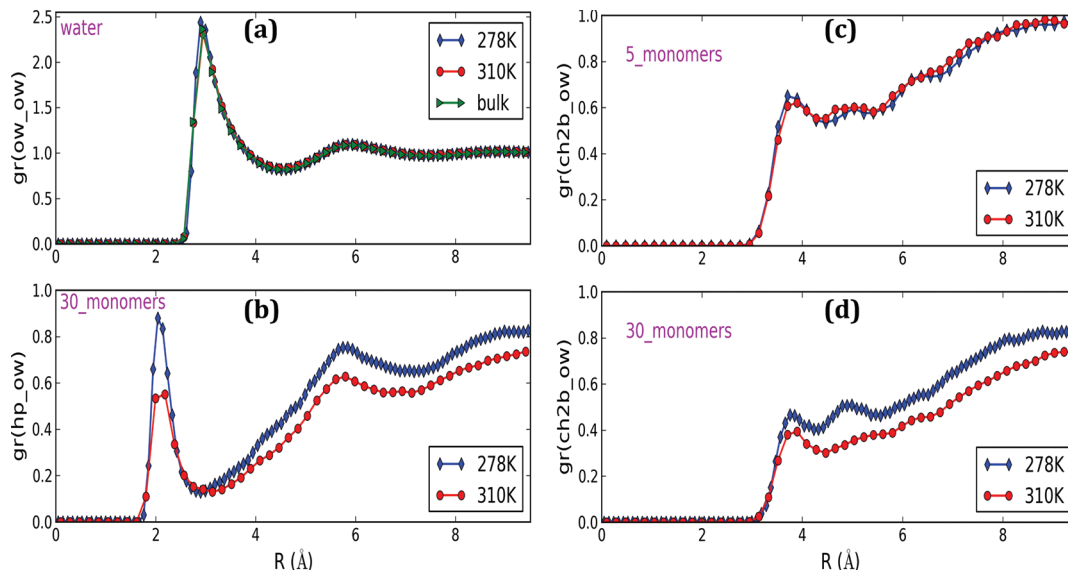


Figure 2. Radial distribution function for (a) ow–ow (oxygen to oxygen atom) in water for a solvated 30-mer PNIPAM as well as bulk water above and below the LCST, (b) hydrogen atom of the amide of the side group (hp) of 30-mer with the water oxygen atom (ow) above and below LCST, (c) carbon atom of the CH_2 of the backbone (ch2b) with the water oxygen atom (ow) for 5-mer above and below LCST, and (d) carbon atom of the CH_2 of the backbone (ch2b) with the water oxygen atom (ow) for 30-mer above and below the LCST.

where VACF represents the velocity autocorrelation function. Such a power spectrum will contain anharmonic contributions as well. To calculate the vibrational spectra, a separate MD simulation was conducted on the final configuration generated at the end of the production run of 18 ns. Simulations were carried out for 100 ps with a time step of 0.5 fs at both 278 and 310 K. Velocities for each atom were stored at every time step. Water molecules were assigned a hydration shell based on their distance from the hydrophilic group of PNIPAM chains (see section III.d). To calculate the VAF for the various shells, water molecules that were present in a given hydration shell at the beginning of the 100 ps simulation runs were assigned to those hydration shells. Thus, water molecules were assigned a hydration shell based on the intermittent definition, i.e., the molecules residing initially in a hydration shell at t_0 are taken into account for calculating the velocity autocorrelation at time $t_0 + t$ even if they have departed from that region in the time interval between t_0 and $t_0 + t$.

It is worth noting that capturing the IR spectra that govern the low-frequency absorption regime is a challenging task for the force-field-based MD simulations.^{61–63} The vibrational spectrum of ambient water is qualitatively well described by force fields above $\sim 300 \text{ cm}^{-1}$; however, the significant resonance at 200 cm^{-1} is either absent or emerges as a weak feature in such simulations.^{62–64} Even the polarizable force fields were not able to capture the prominent peak at 200 cm^{-1} .^{62,64} On the other hand, ab initio MD (AIMD) simulations of the vibrational spectra of water were able to imitate the peak at 200 cm^{-1} , which was assigned to the hydrogen-bonding asymmetric stretching.⁶⁵ The differences in the vibrational spectra obtained by the force-field-based MD simulations and AIMD simulations were explained based on the intermolecular charge fluctuations in locally tetrahedral hydrogen-bond environments.^{66,67} In this work, we mainly focused on the high-frequency region ($> 3000 \text{ cm}^{-1}$) that represents the O–H stretching band of the vibrational spectra.

Although the classical potential models do have limitations in reproducing the electronic contributions and transitions, there

have been several previous works wherein the intensity variations of the intramolecular signals have been used to predict the strength of the hydrogen bonding.²⁷ For example, Ju et al. used molecular dynamics simulations to study a single chain of poly(methacrylic acid) in aqueous solution at various degrees of charge densities.²⁷ In their work, they used the flexible three-centered (F3C) water model. They were successfully able to calculate the vibrational spectra of hydrogen and oxygen atoms of water molecules. They also observed the shift in different bands, namely, libration, bending, and stretching bands, based on the distance of the water molecules from the hydrophilic groups of polymers. They attributed these shifts in the different bands to the strength of hydrogen bonds between water and water and between water and polymer. Tay and Bresme presented MD simulations of gold-passivated nanoparticles in water.⁶⁸ In their work, they used the Toukan–Rahman (TR) flexible water model. The TR potential model is a modified version of the SPC rigid model. In their study, investigation of the vibrational spectrum of interfacial water at the nanoparticle surface supported the existence of free O–H bonds. Similarly, Praprotnik et al. used molecular dynamics (MD) simulations to study the temperature dependence of the bulk water vibrational spectrum.⁶⁹ In their study, they used the flexible simple point charge (SPC) and extended SPC (SPC/E) water models. Praprotnik et al. concluded that both SPC and SPC/E water models could reproduce the experimentally observed effect of temperature on the libration and stretching band of the bulk water. Note that in our study, we used the PCFF water model. Similar to the F3C, TR, SPC, and SPC/E water model, the PCFF water model also has flexible bond and flexible angle terms and hence is expected to give useful insights into the structure and dynamics of water near a polymer undergoing conformational transitions.

III. RESULTS AND DISCUSSION

III.a. Radial Distribution Function (RDF). Figure 2 a shows the RDF for the oxygen–oxygen atom pair in water at 278 and 310 K for a solvated PNIPAM 30-mer as well as pure

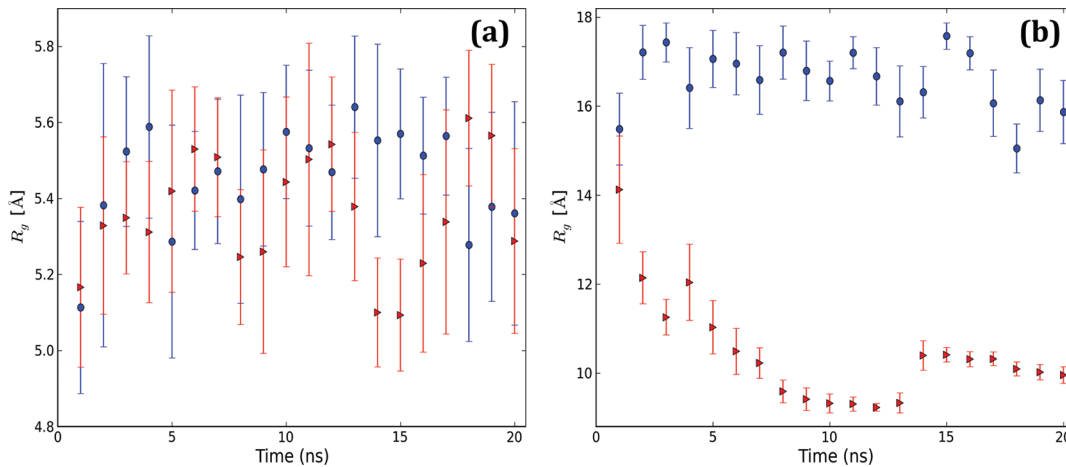


Figure 3. Radius of gyration (R_g) of PNIPAM polymer chains consisting of (a) 5 and (b) 30 monomer units at 278 K (blue circles) and at 310 K (red triangles).

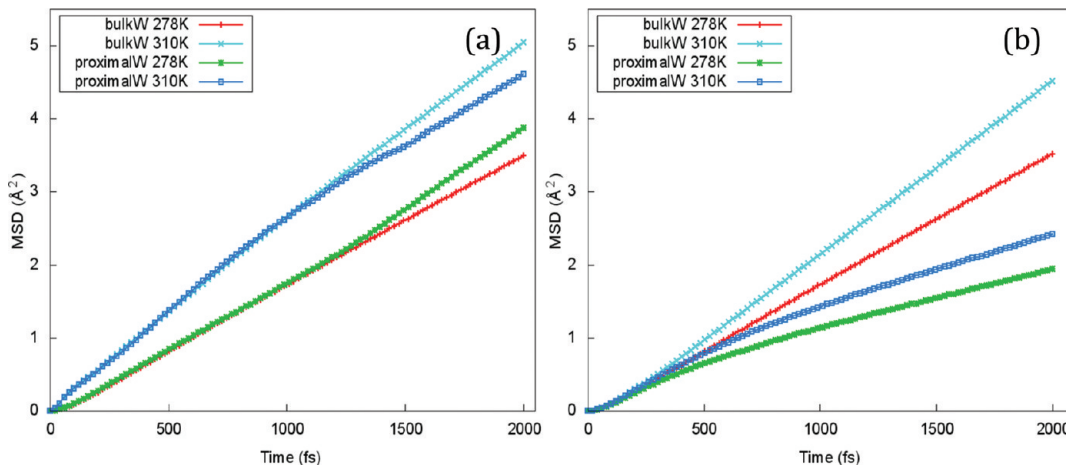


Figure 4. Mean square displacement (MSD) of the oxygen atom of the water molecules present in bulk water and proximal water at 278 and 310 K in the presence of (a) 5-mer and (b) 30-mer.

bulk water. It can be seen that the locations of the first two peaks and trough are the same in all cases. In RDF calculations, the area under the first peak corresponds to the number of water molecules in the first shell surrounding a typical water molecule. The first peak and trough appear at ~ 2.95 and ~ 4.46 Å, respectively, for PNIPAM. Note that the peak height increases slightly in the presence of polymer when compared to pure bulk water. The increase in peak height could be attributed to the increased packing of water molecules in the vicinity of the polymer.

Figure 2b shows the RDF calculations for the hydrogen atom (hp) of the side group of the 30-mer of PNIPAM with the oxygen atom of the water (ow) at 278 and 310 K. This is one of the most favorable atom pairs that is involved in formation of the hydrogen bond between PNIPAM and water. The peak position of the first hydration shell appears at 2.04 Å at both 278 and 310 K. The peak height of both the first and the second peak, however, decreases significantly at 310 K compared to 278 K. The decrease in the peak height of the first and second neighbor peak at 310 K correlates with chain collapse. This is evident from Figure 3b, which shows the R_g of 30-mer at 278 and 310 K. It also suggests that water is expelled from the center of the compact globule structure at 310 K. In other words, the motion of water molecules is restricted at 278

K compared to that at 310 K. This restricted motion of water and interactions between polymer and water (hydrogen-bond formation) may lead to formation of a stable structure for proximal water near the polymer. In this study, the proximal water was defined as the water molecules located in the region that covers the inner part up to the first peak in the RDF of the hydrophilic atom (hydrogen atom of the amide group of PNIPAM or oxygen atom of the carbonyl group of the side group of PNIPAM) with water (oxygen atom of water or hydrogen atom of water). RDF calculations of hp with ow suggest that the region of the proximal water is up to ~ 3 Å.

Figure 2c and 2d shows the RDF calculations for the carbon atom of the CH_2 backbone of 5-mer and 30-mer PNIPAM with the water oxygen atom, respectively, at 278 and 310 K. It can be observed from Figure 2c and 2d that for 5-mer and 30-mer the position of the first peak corresponding to the first hydration shell appears around ~ 3.8 Å at 278 and 310 K. Above the LCST of PNIPAM, however, the peak height is reduced significantly in the case of the 30-mer compared to the 5-mer. In the case of 5-mer, the second peak can be observed both below and above the LCST at ~ 5.0 Å. This second peak is absent in the case of 30-mer PNIPAM at 310 K, which indicates that ordering of water in the second hydration shell near the

polymer backbone is significantly reduced at 310 K (above the LCST of PNIPAM).

III.b. Radius of Gyration (R_g) and Diffusion Coefficient

(D_g). The change in conformations of the 5-mer and 30-mer of PNIPAM at 278 and 310 K is presented in terms of R_g in Figure 3 a and 3b. We did not observe any significant change in the R_g for 5-mer at 310 K compared to 278 K. The mean value of R_g during the production run of 18 ns at 278 and 310 K was 5.5 and 5.4 Å, respectively. This suggests the absence of a coil-to-globule transition in the 5-mer of PNIPAM at 310 K. This is in good agreement with the experimental work carried out by Ahmed et al.⁴⁷ They suggest a “persistant length” of ~10 monomer units for a single PNIPAM chain to show a coil-to-globule transition. In the case of 30-mer, however, we observed a clear difference in the R_g at 310 K compared to the R_g at 278 K. The mean value of the R_g for 30-mer during the production run of 18 ns at 278 K was 16.6 Å, and at 310 K the mean value of R_g decreases to 10.2 Å. This decrement in the mean value of R_g is indicative of a clear coil-to-globule transition.

Figure 4a and 4b shows the mean square displacements (MSDs) of proximal and bulk water at 278 and 310 K for both systems (5-mer and 30-mer) of PNIPAM, respectively. Table 3

Table 3. Self-Diffusion Coefficients for Proximal Water, Bulk Water, and PNIPAM

system	temp. (K)	PNIPAM diffusion coeff. ($10^{-5} \text{ cm}^2/\text{s}$)	proximal water diffusion coeff. ($10^{-5} \text{ cm}^2/\text{s}$)	bulk water diffusion coeff. ($10^{-5} \text{ cm}^2/\text{s}$)
5-mer	278	0.7	6.4	5.6
	310	0.9	7.6	8.0
30-mer	278	0.4	3.0	6.0
	310	0.6	4.0	7.6

lists the diffusion coefficient for the proximal and bulk water and for the carbon atoms in the backbone of the PNIPAM with 5-mer and 30-mer at 278 and 310 K. In the case of 5-mer, it can be clearly seen that the diffusion coefficients of proximal water and bulk water are similar at 278 K. A similar behavior can be observed for 5-mer at 310 K. In the case of 30-mer, at 278 K the diffusion coefficient of the bulk water is two times the diffusion coefficient of the proximal water. This suggests that the proximal water molecules are diffusing slowly as compared to the bulk water. A similar behavior can be observed for 30-mer at 310 K. As expected, the diffusion coefficient of the PNIPAM with 5-mer is faster than the 30-mer at both 278 and

310 K. It can also be seen that the diffusion coefficient of the PNIPAM with both 5-mer and 30-mer is faster at 310 K compared to 278 K.

III.c. Hydrogen-Bonding Characteristics. Hydrogen-bonding characteristics were evaluated using the geometric criteria for hydrogen bonding, as described in section II.b. In the systems studied, the hydrogen bonds between polymer and water were classified into three types based on the donor–acceptor pair: (1) polymer((N–H)–polymer(O=O)), (2) polymer ((N–H)–water(O), and (3) water((O–H)–polymer(O=O)). The results of these analyses both below and above the LCST, by the definition of the intermittent autocorrelation function, are shown in Figure 5a–c.

In the case of type 1 hydrogen bonds, the polymer is both the donor and the acceptor. As shown in Figure 5a, for PNIPAM with 30-mer, the hydrogen-bond correlation decays faster at 278 K compared to 310 K. In the case of 5-mer, we do not observe any significant change in the hydrogen-bond correlations for type 1 hydrogen bonds. The slower decay, observed in the case of 30-mer, at 310 K can be attributed to the globule conformation at 310 K, which leads to strong hydrogen bonding in the polymer. We find a similar behavior in the decay characteristics for hydrogen bonds defined by the continuous correlation function. Comparison of type 2 and 3 interactions, where polymer is donor and acceptor, respectively, suggests that the hydrogen correlation for type 3 (Figure 5c) decays faster when compared to the hydrogen correlation for type 2 (Figure 5b). This slower decay dynamics indicates that the hydrogen bond formed between the carbonyl oxygen (op) and the hydrogen atoms (hw) of water is less stable when compared to the hydrogen bond formed between the hydrogen of the amide group (N(H)) and the water oxygen atom (ow). Figure 5b and 5c represents type 2 and 3 interactions at both below and above the LCST, respectively. We find that the hydrogen-bond correlation decays slowly with an increase in the chain length. This indicates that the hydrogen-bond network formed between PNIPAM with 30-mer and water and between water and water is more stable than the hydrogen-bond network formed between PNIPAM with 5-mer and water and between water and water.

The hydrogen-bond network is dynamic, and the relative populations of the various hydrogen bonds do undergo a change as the polymer undergoes a coil-to-globule transition (see Table 4). Below the LCST, for the 30-mer, the fraction of polymer–water and water–polymer hydrogen bonds are higher

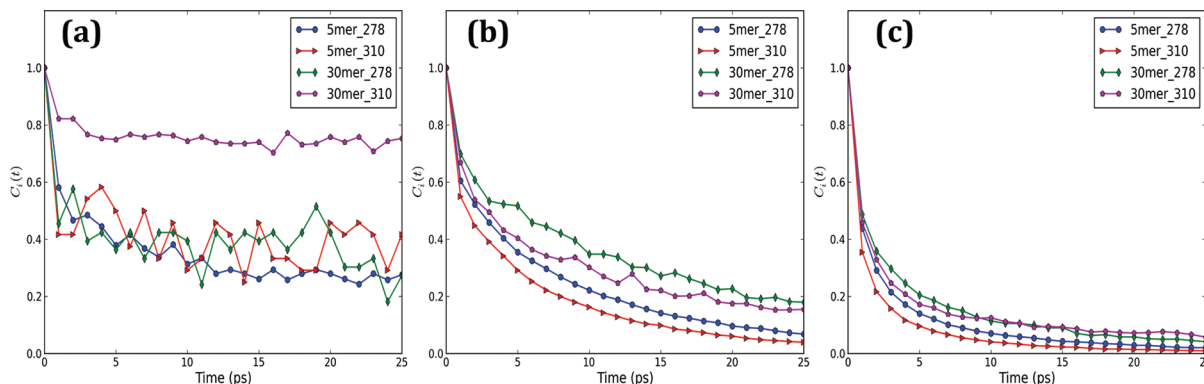


Figure 5. Hydrogen-bond correlations for (a) polymer–polymer (type 1), (b) polymer–water (type 2), and (c) water–polymer (type 3) by intermittent definition at 278 and 310 K.

Table 4. Fractions of Different Types of Hydrogen Bonds Observed during This Study

system	temp. (K)	% of type of bonds		
		polymer–polymer	polymer–water	water–polymer
5-mer	278	0.7	30.5	68.8
	310	1.1	29.8	69.1
30-mer	278	1.3	33.8	64.9
	310	9.7	28.7	61.6

compared to the polymer–polymer hydrogen bonds. Above the LCST, however, the relative fraction of polymer–polymer hydrogen bonds undergoes a significant increase from 1.3% to 9.7% for the case of 30-mer, which undergoes the coil-to-globule transition. The relative populations remain unchanged in the case of 5-mer that does not undergo such a coil-to-globule transition. We note that the population of water–water hydrogen bonds near the hydrophilic and hydrophobic groups is relatively large compared to the polymer–polymer and polymer–water hydrogen bonds and therefore do not undergo a significant change with temperature in both polymers.

The lifetime for hydrogen-bond correlations was defined as the time it takes to reach 37% of the initial value. In this case, the correlation functions are normalized and hence the lifetime is the time taken to reach a value of 0.37. Table 5 lists the decay time for hydrogen-bond correlation for 5-mer and 30-mer.

Table 5. Lifetimes for the Hydrogen-Bond Correlation Function for Type 1, 2, and 3 Hydrogen Bonds at 278 and 310 K

system	bond type	278 K		310 K	
		decay time (ps)	std. dev.	decay time (ps)	std. dev.
5-mer	polymer–polymer (type 1)	~6	0.21	~7	0.19
	polymer–water (type 2)	~5	0.23	~3	0.28
	water–polymer (type 3)	~1	0.39	~1	0.46
30-mer	polymer–polymer (type 1)	~4	0.25	>37	
	polymer–water (type 2)	~10	0.18	~5	0.22
	water–polymer (type 3)	~2	0.36	~1	0.38

The hydrogen-bond lifetimes calculated in our study are comparable to those reported in other polymers and biopolymer.^{70–72} For example, Netz and Dorfmüller studied hydrogel models of polyacrylamide in the presence of the SPC/E water model.⁷² They performed simulations for the hydrogel systems with different concentrations, connectivity characteristics, and pore sizes in order to investigate different polymer environments within the temperature range from 270 to 300 K. In their study, they calculated the hydrogen-bonding lifetimes between polymer and water and between water and water. The hydrogen-bond lifetimes for water molecules present near hydrophilic groups and hydrophobic groups and in bulk were found in the range from ~2 to ~13 ps. Similarly, Bandopadhyay et al. performed atomistic molecular dynamics simulations of an aqueous solution of HP-36 protein to investigate the correlation between the dynamics of the hydration layer water molecules and the lifetimes of hydrogen

bonds between protein and water.⁷¹ In their study, the hydrogen-bond lifetimes between protein and water were found to be in the range from ~14.1 to ~28.6 ps. The hydrogen-bond lifetimes between water and water were found to be in the range from ~2.9 to ~4.7 ps. Balasubramanian et al. studied the dynamics of hydrogen bonds among water molecules themselves and with the polar head groups (PHG) at a micellar surface by molecular dynamics simulations.⁷⁰ Their analyses of individual water molecule trajectories suggested that water molecules can remain bound to the micellar surface in the range from ~3 to ~118 ps.

III.d. Vibrational Spectra of Proximal Water. We now discuss the structural characterization of proximal water using the vibrational spectrum derived from MD simulation trajectories. As mentioned earlier, we define the term “proximal water” to represent water molecules which are located within the region defined by the first peak in the RDF of water molecules and hydrophilic atoms of polymer. The water molecules present in this region can form strong hydrogen bonds with polymer and bind to polymer. Figure 6I and 6II shows the vibrational spectrum for the hydrogen atom of water that is near the PNIPAM at 278 and 310 K, respectively, for both 5-mer and 30-mer. Figure 6a1–a2 and 6b1–b2 shows the corresponding equilibrated structure of PNIPAM and the hydrogen-bond network of water molecules around the polymer. The libration band for proximal water for 5-mer and 30-mer at 278 and 310 K was observed in the region from 0 to 800 cm⁻¹. The bending band for both the 5-mer and the 30-mer was observed in the region from 1500 to 1800 cm⁻¹ at both 278 and 310 K. The high-frequency end of the spectrum (3000–3700 cm⁻¹) typically represents the O–H stretch modes.

As can be clearly seen from Figure 6I, the vibrational spectrum for 5-mer does not show any significant difference for the libration, bending, or stretching band at two different temperatures, namely, at 278 and 310 K. The O–H stretching band for proximal water appears at ~3580 cm⁻¹ at both 278 and 310 K. Note that the O–H stretch modes are strongly correlated to the hydrogen bonding, and the similarity between the vibrational density of states below and above the LCST indicates that thermal perturbations do not significantly disturb the structure of ordered water for a 5-mer PNIPAM.

Comparison of the O–H stretching band for proximal water (~3580 cm⁻¹ in Figure 6I) with those of bulk water (3540 cm⁻¹ at 278 K and 3545 cm⁻¹ at 310 K) suggests that the water–water hydrogen bonds are indeed stronger than the polymer–water hydrogen bonds in the case of 5-mer. The conformational dynamics of small oligomers such as 5-mer is very different from those of larger ones such as 30-mer. In the case of short-chain-length oligomers of PNIPAM such as 3-, 5-, and 10-mer, the chain length of the polymer rapidly fluctuates around the respective mean value of the radius of gyration.³⁷ This behavior is seen at both 278 and 310 K. This observation is in excellent agreement with the recent experimental studies of Ahmed et al. They utilized dynamic light scattering, as well as steady state and time-resolved UV resonance Raman to determine the change in the molecular configurations of the PNIPAM through the LCST.⁷³ On the basis of their spectroscopic data, they suggested that short oligomers such as 3-mer to 10-mer might behave like an “elastic rod” and explore both the coil and the globule configurations with equal probability.⁷³ The solvation cage in these cases is not as stable as in the case of longer polymer chains. Therefore, the water–

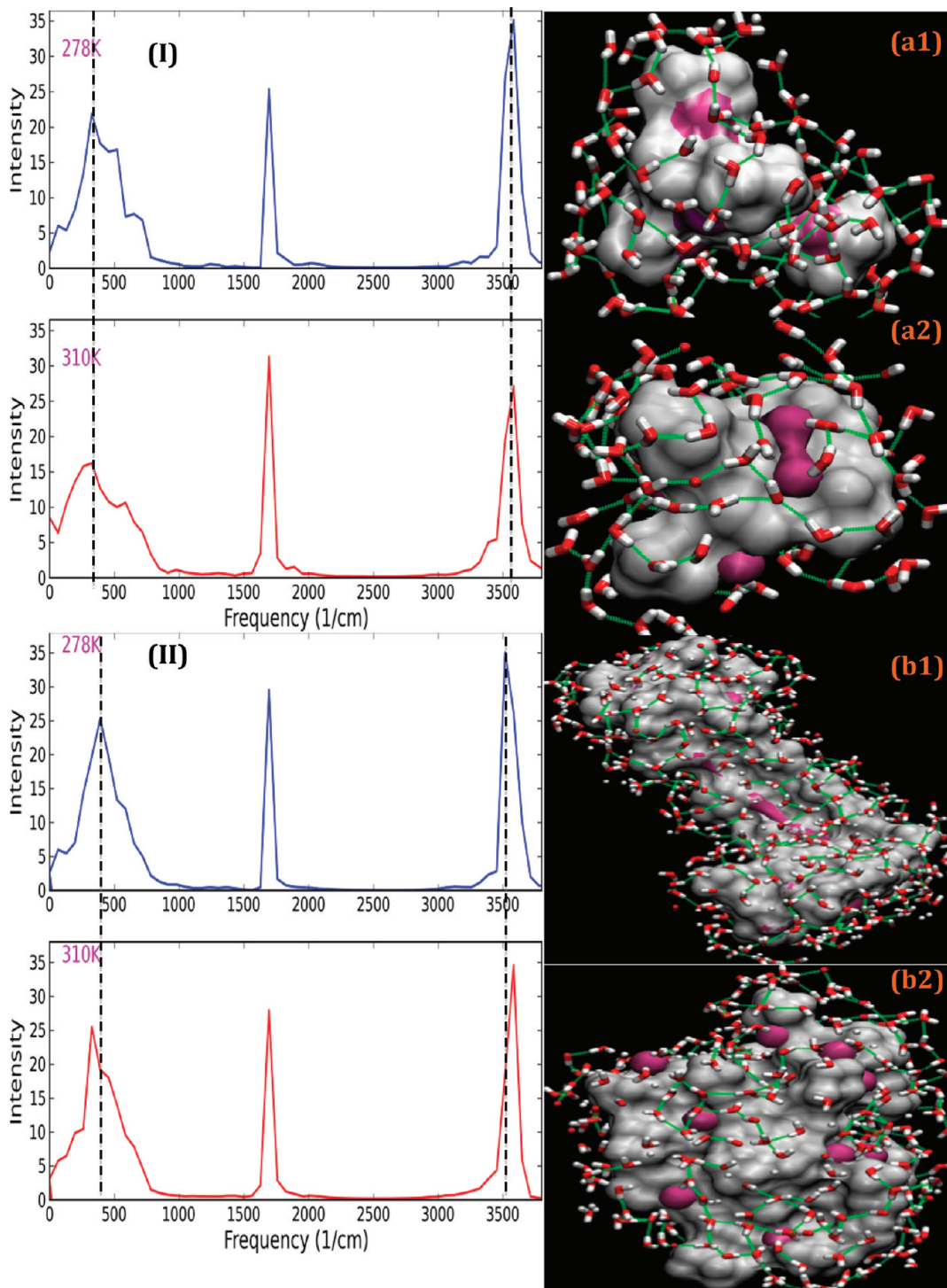


Figure 6. Vibrational spectra of proximal water near the polymer (PNIPAM) (I) 5-mer below and above the LCST and (II) 30-mer below and above the LCST. Side panels a1, a2, b1, and b2 show the snapshot of hydrogen bonding of interfacial water with the polymer for the two cases. It can be seen that the hydrogen-bonding network leads to formation of an ordered solvation structure. This solvation structure remains stable below and above the LCST for 5-mer, whereas it gets disrupted above LCST for 30-mer, which undergoes a coil-to-globule transformation through the LCST.

water hydrogen bonds should be stronger than the polymer–water ones.

As shown in Figure 6II, in the case of proximal water near 30-mer, the libration band shifts significantly toward lower frequency and the peak height for the bending band decreases slightly with increasing temperature. At the high-frequency end of the spectrum, we observe that the O–H stretching band shifts toward higher frequency with an increase in temperature.

At 278 K, the O–H stretching band appears at $\sim 3530 \text{ cm}^{-1}$. At 310 K, however, the stretching band appears at $\sim 3580 \text{ cm}^{-1}$. The red shift in the stretching band at 278 K implies that the hydrogen-bond network between water and polymer is stronger at 278 K compared to that at 310 K.⁴⁵ The red shift observed in the stretching band is in excellent qualitative agreement with the experimental work by Scatena et al.³³ They used TIR VSFS as a molecular probe of the hydrogen bonding and orientation

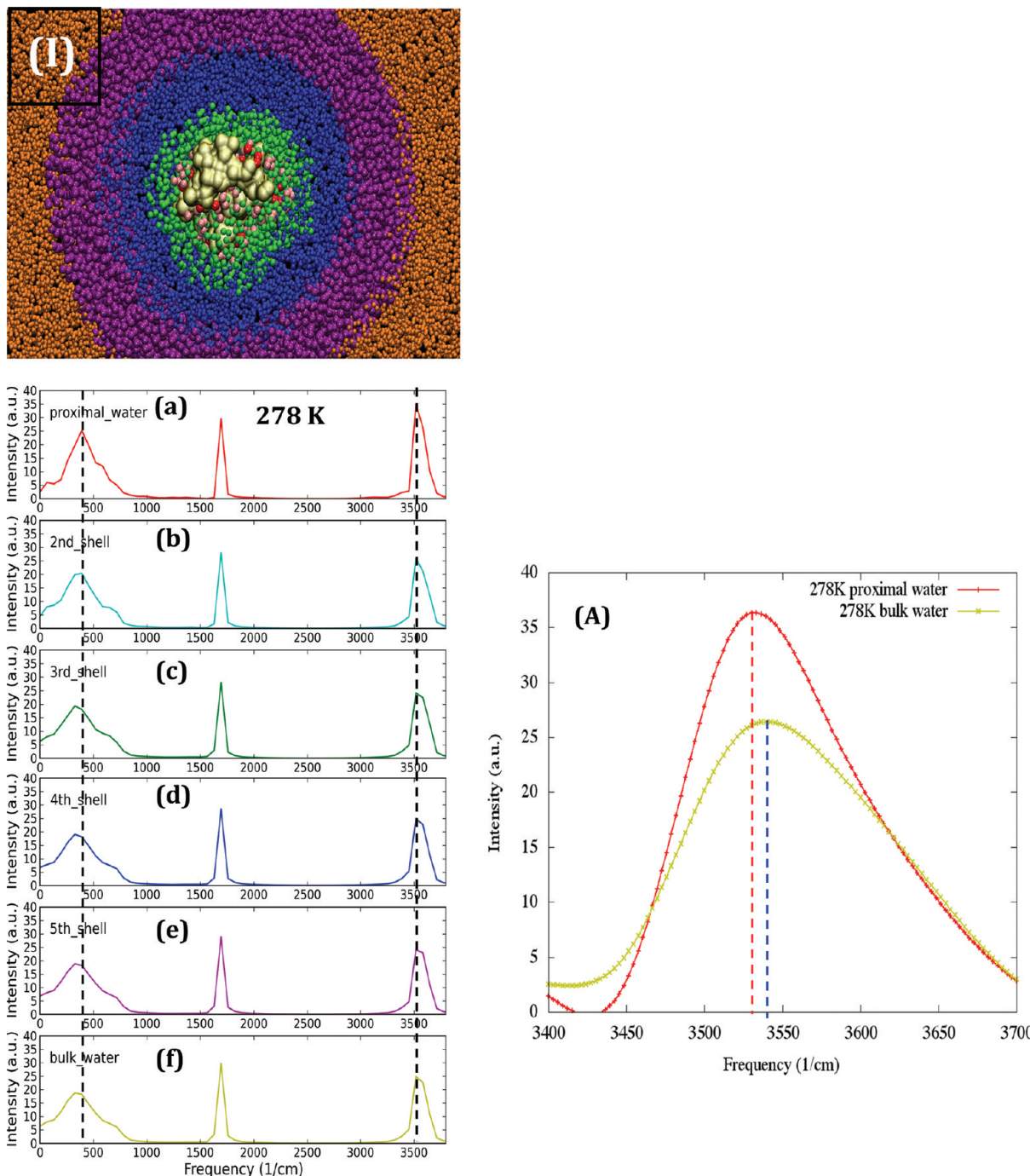


Figure 7. Structural evolution of water characterized by vibrational spectra of hydrogen of water for the various hydration shells in the case of 30-mer below the LCST. Choice of the various regions below the LCST is depicted in the simulation snapshots shown in I. First peak in the RDF between hydrophilic groups and water is used to define a region within which water molecules can form strong hydrogen bonds with other water molecules and with the various groups in the polymer chain: (a) Proximal water and (f) the bulk below the LCST. Intermittent panels b–e correspond to vibrational spectra obtained below the LCST for regions located increasingly away from the polymer, eventually transforming into bulk spectra shown in f. (A) Zoomed in plot of proximal water and bulk water below the LCST (namely, at 278 K).

of interfacial water molecules at organic/water interfaces and at the vapor/water interface. They observed a red shift with an increase in the strength of the hydrogen bonds. A similar red shift was observed in the presence of strong hydrogen bonds in several other experimental studies carried out on the vibrational spectrum of water at liquid/water, vapor/water, quartz/water, etc., interfaces.^{34,36,74} The O–H stretch band of the proximal water of 30-mer of PNIPAM suggests the presence of stronger hydrogen-bonding between 30-mer of PNIPAM and proximal

water at 278 K ($\sim 3530 \text{ cm}^{-1}$) as compared to the hydrogen bonds between 5-mer and proximal water at 278 K ($\sim 3580 \text{ cm}^{-1}$). The presence of the weaker hydrogen bonding between 5-mer of PNIPAM and water molecules could be one of the reasons for the absence of a coil-to-globule transition in the 5-mer.

Inspection of simulation trajectories suggests that water molecules form hydrogen bonds with hydrophilic groups of PNIPAM side chains (amide and carbonyl groups) both below

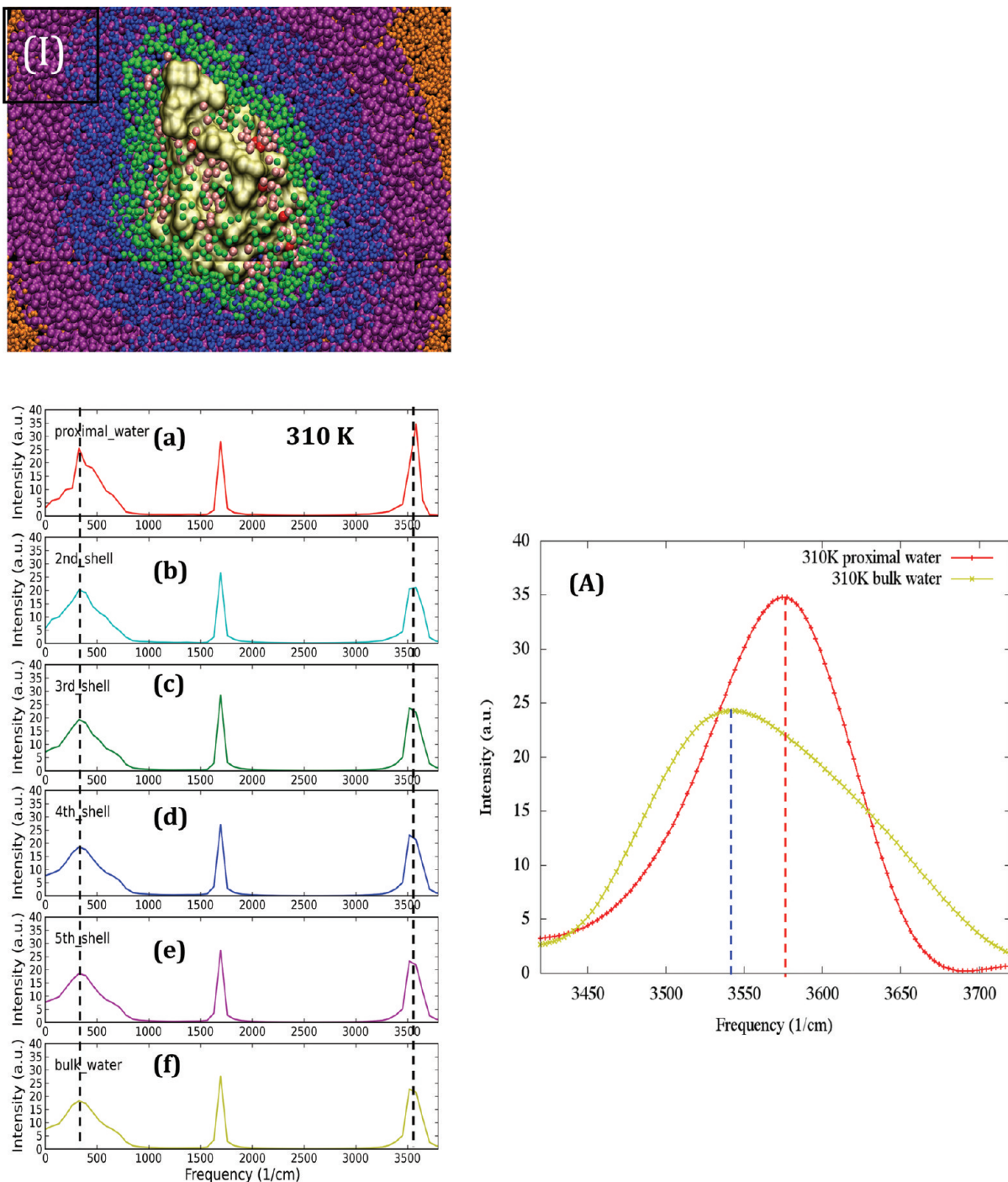


Figure 8. Structural evolution of water characterized by vibrational spectra of hydrogen of water for the various hydration shells in the case of 30-mer above the LCST. Choice of the various regions above the LCST is depicted in the simulation snapshots shown in II: (a) proximal water and (f) the bulk above the LCST. Intermittent panels b–e correspond to vibrational spectra obtained above the LCST for regions located increasingly away from the polymer, eventually transforming into bulk spectra shown in f. (A) Zoomed in plot of proximal water and bulk water above the LCST (namely, at 310 K).

and above the LCST. However, below the LCST, water molecules near the hydrophobic groups of PNIPAM side chains rearrange themselves to form hydrogen bonds among themselves as they cannot form a hydrogen bond with hydrophobic groups.²⁸ This leads to formation of stable network of hydrogen-bond bridges of water molecules between adjacent and alternate monomers of PNIPAM. This hydrogen-bond network between water and polymer and between water and water keeps the polymer solvated below the LCST. At

elevated temperatures, however, the hydrogen-bond network between water and water is no longer stable and gets disrupted.²⁸ This leads to destruction of the hydrogen-bond network of the water molecules between alternate and adjacent side groups of PNIPAM, and this results in collapse of PNIPAM. The presence of the hydrogen-bond bridges between water and water could lead to formation of very strong and stable hydrogen bonds between water and polymer below the LCST compared to above the LCST. This might explain the

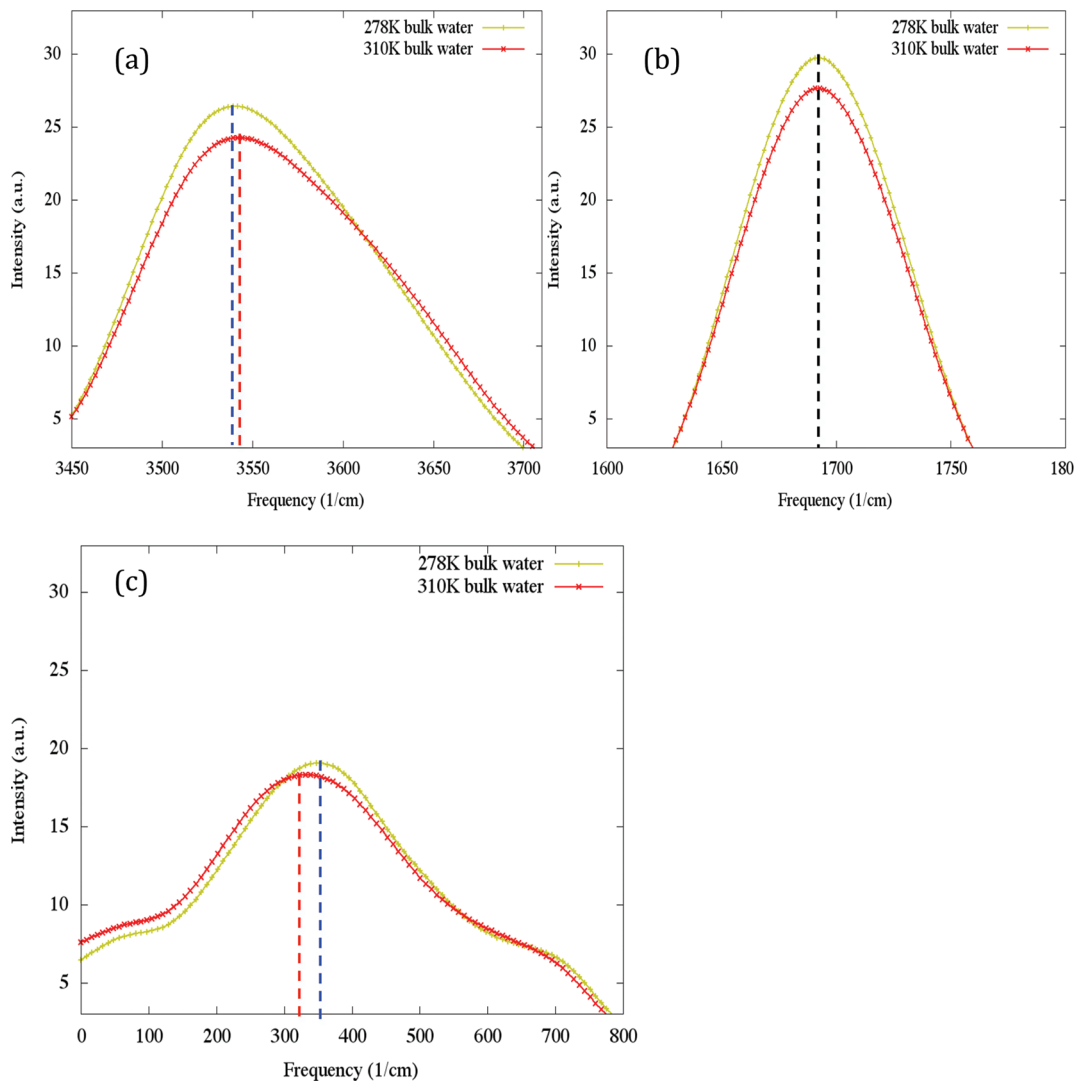


Figure 9. Spectra of bulk water for PCFF model at 278 and 310 K: (a) stretching band, (b) bending band, and (c) libration band.

red shift observed in the stretching band of O–H spectra below the LCST compared to above the LCST.

To further explore the hydrogen-bonding characteristics of water with PNIPAM 30-mer we also studied the vibrational spectrum of water as a function of distance from the PNIPAM chain. We classified the hydrogen and oxygen atoms of water molecules based on the distance between the hydrophilic atoms of the polymer and the hydrogen or oxygen atom of water. In other words, hydrogen atoms of water were placed in the respective shell based on its distance from the oxygen atom of the carbonyl group of the polymer side group. Oxygen atoms of water molecules were classified based on their distance from the hydrogen atom of the amide group of the polymer side group. The hydrogen and oxygen atoms of water in the system were classified as (a) proximal water based on the RDF of hydrophilic atoms of PNIPAM with water molecules (hydrogen atoms of water within 2 Å of the oxygen atom of the carbonyl group of the PNIPAM side group and the oxygen atom of water within 3 Å of the hydrogen atom of the amide group of the PNIPAM side group), (b) second hydration shell (hydrogen atoms of water within 2–5 Å of the oxygen atom of the carbonyl group of the PNIPAM side group and the oxygen atom of water within 3–5 Å of the hydrogen atom of the amide

group of the PNIPAM side group), (c) third hydration shell (within 5–10 Å), (d) fourth hydration shell (within 10–20 Å), (e) fifth hydration shell (within 20–30 Å), (f) bulk water. Figures 7I and 8I show the snapshot of polymer and different hydration shells at 278 and 310 K, respectively. Figures 7a–f and 8a–f show the vibrational spectrum due to hydrogen atoms in different hydration shells at 278 and 310 K, respectively. Figures 7A and 8A show the zoomed in plot of the vibrational spectrum due to hydrogen atoms of proximal water and bulk water at 278 and 310 K, respectively.

As can be seen from Figures 7a–f and 8a–f, the vibrational spectra at 278 and 310 K in the first hydration shell are significantly different from each other as well as that of bulk water. At 278 K, the stretching band, which is characteristic of hydrogen bonds, for the proximal water and bulk water appears at ~ 3530 and ~ 3540 cm $^{-1}$, respectively (see Figure 7 A). The slight red shift observed in the O–H stretching band of proximal water suggests the presence of stronger hydrogen bonds in proximal water and PNIPAM as compared to the bulk water. We also observe that the peak height decreases as we move away from the polymer toward the bulk water at 278 K. A slight broadening of the stretching band peak for bulk water as compared to proximal water can also be noticed in Figure 7 A.

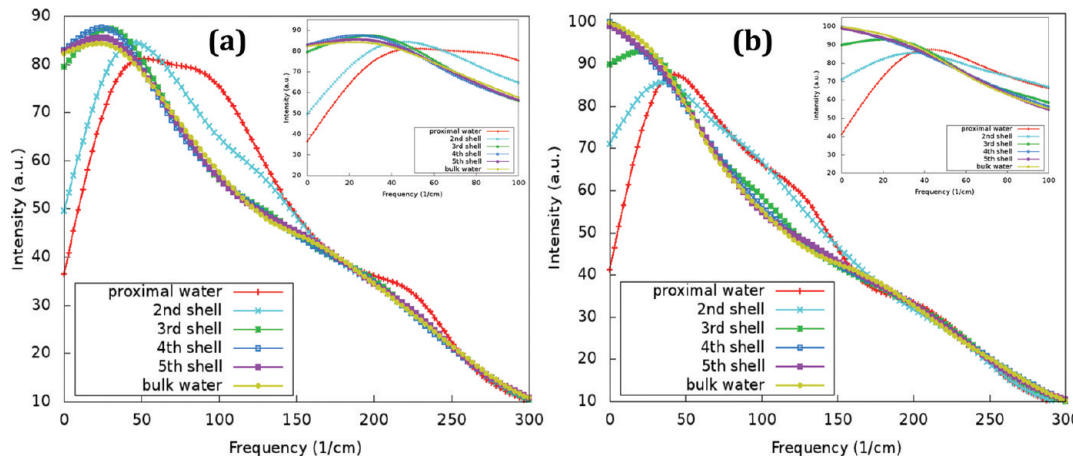


Figure 10. (a and b) Structural evolution of proximal water characterized by vibrational spectra of the oxygen atom of water for the various hydration shells in the case of 30-mer above and below the LCST. Choice of the various regions is the same as that depicted in section III.d.

This suggests the presence of strong hydrogen bonds between PNIPAM and proximal water as compared to the hydrogen bonds that exist in bulk water with itself. The peak height for the bending band ($\sim 1690\text{ cm}^{-1}$) in the vibrational spectrum at 278 K reduces as we move away from the PNIPAM chain and approach that of the bulk water. It can also be observed that the libration peak at 278 K in proximal water shows a blue shift (391 cm^{-1}) compared to bulk water (355 cm^{-1}).

At 310 K, as can be seen in Figure 8 A, stretching band of proximal water (3580 cm^{-1}) shows a blue shift compared to the bulk water (3545 cm^{-1}). This indicates that there exists a hydrogen-bond network between polymer and water above the LCST (310 K), which is different and weaker than the bulk water. In the case of libration (326 cm^{-1}) and bending band (1690 cm^{-1}) of the proximal and bulk water, at 310 K, we do not observe any significant change in the peak positions. The peak height for the libration band, however, decreases as we move away from polymer and approach bulk water.

To study the effect of temperature on the vibrational spectra, we now compare the vibrational spectra of bulk water at 278 and 310 K. Figure 9a, 9b, and 9c shows the stretching, bending, and libration bands of the vibrational spectra of bulk water (PCFF water model) at 278 and 310 K. A small blue shift from ~ 3540 to $\sim 3545\text{ cm}^{-1}$ can be observed in the O–H stretching band when the temperature is raised from 278 to 310 K. The O–H libration band also shows a slight blue shift at 278 K to $\sim 355\text{ cm}^{-1}$ compared to $\sim 326\text{ cm}^{-1}$ at 310 K. This suggests that the hydrogen-bond network in bulk water, as expected, is stronger at 278 K compared to that at 310 K. Moreover, we do observe narrowing of the O–H bending band of PCFF bulk water at $\sim 1690\text{ cm}^{-1}$ as the temperature is increased from 278 to 310 K. Similar observations were made in the experimental studies by Maréchal et al.⁷⁵ Maréchal et al. implemented an ATR (attenuated total reflection) setup to calculate the IR spectra of water for wavenumbers higher than $\sim 700\text{ cm}^{-1}$. In their experimental study, they recorded the spectra at every 5 °C for temperatures ranging between -5 to 80 °C. They observed narrowing in the O–H bending band that was observed at $\sim 1650\text{ cm}^{-1}$ with increasing temperature for pure water. In another study, Praprotnik et al. used MD simulations to study the temperature dependence of the bulk water vibrational spectrum.⁶⁹ In their study, they used SPC and SPC/E water models. As mentioned earlier in our study, we used the PCFF water model. Similar to the SPC and SPC/E water

model, the PCFF water model also has flexible bond and flexible angle terms. Praprotnik et al. carried out MD simulations at -4.0 and 80 °C and calculated the vibrational spectra for both water models. They observed a slight blue shift in the stretching band when temperature was raised from -4 to 80 °C. Praprotnik et al. concluded that both SPC and SPC/E water models could reproduce the experimentally observed effect of temperature on the libration and stretching band of bulk water. However, both SPC and SPC/E water models could not reproduce the experimentally observed effect of temperature by Maréchal et al. on the bending band of the bulk water. In our study, although the magnitude of the shifts is small, they are consistent with that reported in the experimental study by Maréchal et al. and the theoretical study by Praprotnik et al.⁶⁹ Note that the temperature increase in our case is very modest compared to those in the previous studies mentioned above, and hence, the differences are not expected to be very significant.

We also measured the vibrational spectrum for the oxygen atom of water molecules at 278 and 310 K. The spectrum corresponding to the oxygen of water has two characteristic features: a peak at low frequencies (centered at $\sim 40\text{--}50\text{ cm}^{-1}$) representing the O–O–O intermolecular bending motions of H-bonded molecules and a shoulder at $\sim 220\text{ cm}^{-1}$ resulting from the O–O intermolecular stretching mode.^{75–77}

The low-frequency vibrational spectrum representing the O–O–O intermolecular bending for different hydration shells at 278 and 310 K is shown in Figure 10a and 10b, respectively. At both 278 and 310 K for the proximal water, we observe a prominent peak at $\sim 40\text{--}50\text{ cm}^{-1}$. At both simulated temperatures, we observe a blue shift in the O–O–O intermolecular bending peak as we go from proximal water toward the bulk. We also note that the peak is broader at 278 K compared to 310 K. The blue shift is a consequence of the distortion of the tetrahedral order in proximal water caused by lateral diffusion being reduced and also by changes in the distribution of H bonds. A similar blue shift in the low-frequency oxygen spectra was also observed in interfacial water present in micellar solutions.⁷⁶

Additionally, as stated earlier, we also observe a prominent shoulder at $\sim 220\text{ cm}^{-1}$ for proximal water at 278 K compared to 310 K. At 278 K, the shoulder observed at $\sim 220\text{ cm}^{-1}$ becomes red shifted as we go away from PNIPAM toward bulk water. As reported in refs 27 and 76–78, this means that a

stronger hydrogen-bonding network is present in proximal water near the PNIPAM chain as compared to bulk water at 278 K. In the case of the $\sim 220\text{ cm}^{-1}$ band, at 310 K, we do not see any significant change in the shoulder as we move from proximal water to bulk water. On the other hand, the OH stretching signal at 310 K in Figure 8a2–f2 is blue shifted, which does suggest that the bulk water hydrogen bonds are stronger than the polymer–water hydrogen bonds. This blue shift in the OH stretching peak is also expected since the polymer is now in a collapsed state having undergone the coil-to-globule transition. To explain this difference between the OH stretching peaks (Figure 8A) and the O···O stretching peaks (Figure 10b) at 310 K, we note that the peak near 200 cm^{-1} is related to the interaction-induced effects as pointed out by Madden and co-workers and also observed in Raman and inelastic neutron scattering.^{63,77,79–83} This peak is assigned to the O···O stretching mode of the O–H···O unit. If the water molecules were not polarizable (as is the case in the classical potential model utilized in this work), the band at $\sim 200\text{ cm}^{-1}$ corresponding to the intermolecular vibrations would not strongly affect the dielectric relaxation and, as a result, would not completely capture the dipole-induced dipole mechanics. This band has been shown to be weak in several previous molecular dynamics simulations.^{63,77,79–83} The intermolecular vibrations and extended hydrogen-bond network would continue to exist even in the absence of polarizability. As pointed out by these prior MD simulation studies, the O–H stretching peak would more accurately capture the differences in the hydrogen-bonding network.^{27,69}

IV. CONCLUSION

We employed MD simulations to study a fully atomistic model of PNIPAM chains in water. The simulation trajectories were used to obtain the vibrational spectra and characterize the interactions between PNIPAM and water and between water and water both below and above the LCST of PNIPAM (at 278 and 310 K, respectively). We find that the 5-mer of PNIPAM does not show an LCST. Analysis of the various structural and dynamical correlations suggests that there exists a quasi-stable structure for proximal water at both 278 and 310 K for the 5-mer. The structure of the hydrogen-bonding network around the solvated 5-mer PNIPAM chain remains in place as the temperature is increased from 278 to 310 K. We find that the 30-mer of PNIPAM exhibits a coil-to-globule transition above the experimental LCST. Our analysis of the calculated vibrational spectrum of water suggests that the structure and strength of hydrogen bonds between PNIPAM and proximal water and between water and water is significantly different below and above the observed LCST for 30-mer. A red shift in the stretching modes of the hydrogen atom of proximal water (H–O bond) spectra at 278 K suggests very strong hydrogen bonding between PNIPAM and proximal water compared to hydrogen bonding between PNIPAM and proximal water at 310 K. Similarly, the libration band for proximal water shows a red shift when the temperature is increased from 278 to 310 K. The calculated vibrational spectra for water molecules in different hydration shells of PNIPAM at 278 and 310 K are used to evaluate the degree of stability of the hydrogen-bond network formed by proximal water. We observe that below the LCST the strength of the hydrogen bonds is strongest when close to the PNIPAM and weaker as one moves toward bulk water. Above the LCST, the 30-mer is in a collapsed state and hence the hydrogen-bond strength is stronger for bulk water as

compared to proximal water. The dynamics of the structural stability and hydrogen-bonding network can be characterized by the observed peak intensities and frequency shifts at the low-(libration and bending modes) and high-frequency (stretching modes) ends of the spectra. The results of this simulation study lay the groundwork for experimentally probing the role and structure of proximal water in defining the transport properties of complex systems like biopolymers and hydrogels. These results also develop an atomic-scale picture of proximal water that can have important implications for several natural and technological processes, including interfacial polymerization, molecular transport, chemical assemblies, and macromolecular folding and assembly.

■ AUTHOR INFORMATION

Corresponding Author

*E-mail: skrssank@anl.gov (S.K.R.S.S.); mancini@anl.gov (D.C.M.).

Notes

The authors declare no competing financial interest.

■ ACKNOWLEDGMENTS

Use of the Center for Nanoscale Materials was supported by the U.S. Department of Energy, Office of Science, Office of Basic Energy Sciences, under Contract No. DE-AC02-06CH11357. The authors acknowledge useful discussions with Dr. Kamlesh Suthar and Dr. Zheng Li.

■ REFERENCES

- (1) Wang, J.; Kalinichev, A.; Kirkpatrick, R. J.; Cygan, R. T. *J. Phys. Chem. B* **2005**, *109*, 15893.
- (2) Lee, S. H.; Rossky, P. J. *J. Chem. Phys.* **1994**, *100*, 3334.
- (3) Buuren, A. R. v.; Marrink, S. J.; Berendsen, H. J. C. *J. Phys. Chem.* **1993**, *97*, 9206.
- (4) Bhattacharyya, S. M.; Wang, Z.-G.; Zewail, A. H. *J. Phys. Chem. B* **2003**, *107*, 13218.
- (5) Bizzarri, A. R.; Cannistraro, S. *J. Phys. Chem. B* **2002**, *106*, 6617.
- (6) Tarek, M.; Tobias, D. J. *Phys. Rev. Lett.* **2002**, *88*, 138101.
- (7) Kerisit, S.; Cooke, D. J.; Spagnoli, D.; Parker, S. C. *J. Mater. Chem.* **2005**, *15*, 1454.
- (8) Davis, J. A.; Kent, D. B. *Rev. Mineral.* **1990**, *23*, 177.
- (9) Brown, G. E. *Science* **2001**, *294*, 67.
- (10) Brown, G. E.; Parks, G. A. *Int. Geol. Rev.* **2001**, *43*, 963.
- (11) Wang, J.; Kalinicheva, A. G.; Kirkpatrick, R. J. *Geochim. Cosmochim. Acta* **2006**, *70*, 562.
- (12) Hartnig, C.; Witschel, W.; Spohr, E. *J. Phys. Chem. B* **1998**, *102*, 1241.
- (13) Pal, S. K.; Zhao, L.; Zewail, A. H. *Proc. Natl. Acad. Sci. U.S.A.* **2003**, *100*, 8113.
- (14) Smolyreva, A. M.; Voth, G. A. *Biophys. J.* **2002**, *82*, 1460.
- (15) Garofalini, S. H. *J. Non-Cryst. Solids* **1990**, *120*, 1.
- (16) Hochella, M. F.; White, A. F. *Rev. Mineral.* **1990**, *23*, 1.
- (17) Rustad, J. R.; Felmy, A. R.; Bylaska, E. J. *Geochim. Cosmochim. Acta* **2003**, *67*, 1001.
- (18) Dickinson, E. *Colloids Surf., B* **1999**, *15*, 161.
- (19) Umezawa, K.; Morikawa, R.; Nakamura, H.; Higo, J. *J. Chem. Phys.* **2010**, *132*, 155103.
- (20) Chakraborty, S.; Sinha, S. K.; Bandyopadhyay, S. *J. Phys. Chem. B* **2007**, *111*, 13626.
- (21) Sinha, S. K.; Chakraborty, S.; Bandyopadhyay, S. *J. Phys. Chem. B* **2008**, *112*, 8203.
- (22) Chakraborty, S.; Bandyopadhyay, S. *J. Phys. Chem.* **2007**, *111*, 7626.
- (23) Jana, M.; Bandyopadhyay, S. *Langmuir* **2010**, *26*, 14097.
- (24) Guo, J.; Xiab, F.; Wub, Y.; Qua, X.; Yanga, Z.; Jiangb, L. *J. Controlled Release* **2007**, *117*, 396.

- (25) Numata, K.; Katashima, T.; Sakai, T. *Biomacromolecules* **2011**, *12*, 2137.
- (26) Jamadagni, S. N.; Godawat, R.; Garde, S. *Langmuir* **2009**, *25*, 13092.
- (27) Ju, S.-P.; Lee, W.-J.; Huang, C.-I.; Cheng, W.-Z.; Chung, Y.-T. *J. Chem. Phys.* **2007**, *126*, 224901.
- (28) Schild, H. G. *Prog. Polym. Sci.* **1992**, *17*, 163.
- (29) McGuire, J. A.; Shen, Y. R. *Science* **2006**, *313*, 1945.
- (30) Wei, X.; Shen, Y. R. *Phys. Rev. Lett.* **2001**, *86*, 4799.
- (31) Miranda, P. B.; Shen, Y. R. *J. Phys. Chem. B* **1999**, *103*, 3292.
- (32) Du, Q.; Freysz, E.; Shen, Y. R. *Science* **1994**, *264*, 826.
- (33) Scatena, L. F.; Brown, M. G.; Richmond, G. L. *Science* **2001**, *292*, 908.
- (34) Du, Q.; Superfine, R.; Freysz, E.; Shen, Y. R. *Phys. Rev. Lett.* **1993**, *70*, 2313.
- (35) Ostroverkhov, V.; Waychunas, G. A.; Shen, Y. R. *Phys. Rev. Lett.* **2005**, *94*, 046102.
- (36) Du, Q.; Freysz, E.; Shen, Y. R. *Phys. Rev. Lett.* **1994**, *72*, 238.
- (37) Deshmukh, S. A.; Sankaranarayanan, S. K. R. S.; Suthar, K.; Mancini, D. C. *J. Phys. Chem. B* **2012**, DOI: 10.1021/jp210788u.
- (38) Patel, A. J.; Varilly, P.; Jamadagni, S. N.; Acharyaa, H.; Gardea, S.; Chandler, D. *Proc. Natl. Acad. Sci., U.S.A.* **2011**, *108*, 17678.
- (39) Li, I. T. S.; Walker, G. C. *J. Am. Chem. Soc.* **2010**, *132*, 6530.
- (40) Dobrynin, A. V.; Rubinstein, M.; Obukhov, S. P. *Macromolecules* **1996**, *29*, 2974.
- (41) Giuseppina, R.; Fabio, G. *J. Biomed. Mater. Res., Part A* **2010**, *92*, 1382.
- (42) Pickett, G. T.; Balazs, A. C. *Langmuir* **2001**, *17*, 5111.
- (43) Halperin, A.; Zhulina, E. B. *Macromolecules* **1991**, *24*, 5391.
- (44) Garde, S.; Patel, A. J. *Proc. Natl. Acad. Sci., U.S.A.* **2011**, *108*, 16491.
- (45) Dybal, J.; Trchová, M.; Schmidt, P. *Vibr. Spectrosc.* **2009**, *51*, 44.
- (46) Sun, H.; Mumby, S. J.; Maple, J. R.; Hagler, A. T. *J. Am. Chem. Soc.* **1994**, *116*, 2978.
- (47) Zeeshan, A.; Gooding, E.; Pimenov, K.; Wang, L.; Asher, S. A. *J. Phys. Chem. B* **2009**, *114*, 4248.
- (48) Fritz, L.; Hofmann, D. *Polymer* **1997**, *38*, 1035.
- (49) Maple, J. R.; Thacher, T. S.; Dinur, U.; Hagler, A. T. *Chem. Des. Autom. News* **1990**, *5*, 5.
- (50) Sun, H. *J. Comput. Chem.* **1994**, *15*, 752.
- (51) Plimpton, S. *J. Comput. Phys.* **1995**, *117*, 1.
- (52) Allen, M. P.; Tildesley, D. J. *Computer Simulations of Liquid*; Clarendon Press: Oxford, 1987.
- (53) Maeda, Y.; Nakamura, T.; Ikeda, I. *Macromolecules* **2002**, *35*, 10172.
- (54) Wu, C.; Wang, X. *Phys. Rev. Lett.* **1998**, *80*, 4092.
- (55) Tamai, Y.; Tanaka, H. *Macromolecules* **1996**, *29*, 6761.
- (56) Luzar, A.; Chandler, D. *J. Chem. Phys.* **1993**, *98*, 8160.
- (57) Zichi, D. A.; Rossky, P. J. *J. Chem. Phys.* **1985**, *83*, 797.
- (58) Rossky, P. J.; Zichi, D. A. *Faraday Symp. Chem. Soc.* **1982**, *17*, 69.
- (59) Ladanyi, B. M.; Skaf, M. S. *Ann. Rev. Phys. Chem.* **1993**, *44*, 335.
- (60) Rapaport, D. C. *Mol. Phys.* **1983**, *50*, 1151.
- (61) Heyden, M.; Sun, J.; Funkner, S.; Mathias, G.; Forbert, H.; Havenith, M.; Marx, D. *Proc. Natl. Acad. Sci., U.S.A.* **2010**, *107*, 12068.
- (62) Harder, E.; Eaves, J. D.; Tokmakoff, A.; Berne, B. J. *Proc. Natl. Acad. Sci., U.S.A.* **2005**, *102*, 11611.
- (63) Madden, P. A.; Impey, R. W. *Chem. Phys. Lett.* **1986**, *123*, 502.
- (64) Fanourgakis, G. S.; Xantheas, S. S. *J. Chem. Phys.* **2008**, *128*, 074506.
- (65) Silvestrelli, P. L.; Bernasconi, M.; Parrinello, M. *Chem. Phys. Lett.* **1997**, *277*, 478.
- (66) Sharma, M.; Resta, R.; Car, R. *Phys. Rev. Lett.* **2005**, *95*, 187401.
- (67) Chen, W.; Sharma, M.; Resta, R.; Galli, G.; Car, R. *Phys. Rev. B* **2008**, *77*, 245114.
- (68) Tay, K.; Bresme, F. *J. Mater. Chem.* **2006**, *16*, 1956.
- (69) Praprotnik, M.; Janežič, D.; Mavri, J. *J. Phys. Chem. A* **2004**, *108*, 11056.
- (70) Balasubramanian, S.; Pal, S.; Bagchi, B. *Phys. Rev. Lett.* **2002**, *89*, 115505.
- (71) Bandyopadhyay, S.; Chakraborty, S.; Bagchi, B. *J. Am. Chem. Soc.* **2005**, *127*, 16660.
- (72) Netz, P. A.; Dorfmüller, T. *J. Phys. Chem. B* **1996**, *102*, 4875.
- (73) Ahmed, Z.; Gooding, E.; Pimenov, K.; Wang, L.; Asher, S. J. *Phys. Chem. B* **2009**, *113*, 4248.
- (74) Benjamin, I. *Phys. Rev. Lett.* **1994**, *73*, 2083.
- (75) Maréchal, Y. *J. Mol. Struct.* **1994**, *322*, 105.
- (76) Pal, S.; Balasubramanian, S.; Bagchi, B. *Phys. Rev. E* **2003**, *67*, 061502.
- (77) Martí, J.; Padro, J. A.; Guàrdia, E. *J. Chem. Phys.* **1996**, *105*, 639.
- (78) Padro, J. A.; Martí, J.; Guardia, E. *J. Phys.: Condens. Matter* **1994**, *6*, 2283.
- (79) Impey, R. W.; Madden, P. A.; McDonald, R. W. *Mol. Phys.* **1982**, *40*, 515.
- (80) Madden, P. A. *Molecular Liquids: Dynamics and Interactions*; Reidel: Dordrecht, 1984.
- (81) Nemethy, G.; Scheraga, H. *J. Chem. Phys.* **1964**, *41*, 680.
- (82) See the articles in *Water: A Comprehensive Treatise*; Plenum: New York, 1972.
- (83) See the articles in *The Structure and Properties of Water*; Oxford University Press: London, 1969.